Northumbria Research Link

International Journal of Numerical Methods for He
Flui

Influence of curvature distribution smoothing on the reduction of aerofoil self-noise

SCHOLARONE™
Manuscripts

Influence of curvature distribution smoothing on the reduction of aerofoil self-noise

Xiang Shen, Northumbria University

Eldad Avital, Queen Mary University of London

Zaheer Ikram, Defence Science and Technology Laboratory Portsmouth

Liming Yang, Nanjing University of Aeronautics and Astronautics

Theodosios Korakianitis, Saint Louis University

Laurent Dala, Northumbria University

ABSTRACT

Purpose – The paper aims to investigate the influence of smooth curvature distributions on the self-noise of a low Reynolds number aerofoil and to unveil the flow mechanisms in the phenomenon.

Design/methodology/approach – The paper performed Large Eddy Simulation (LES) approach to investigate the unsteady aerodynamic performance of both the original aerofoil E387 and the redesigned aerofoil A7 in a time-dependent study of boundary layer characteristics at Reynolds number 100,000 and Angle of Attack 4-degree. The aerofoil A7 is redesigned from E387 by removing the irregularities in the surface curvature distributions and keeping a nearly identical geometry. Flow vorticity magnitude of both aerofoils, along with the spectra of the vertical fluctuating velocity component and noise level, are analysed to demonstrate the bubble flapping process near the trailing edge and the vortex shedding phenomenon.

Findings – The paper provides quantitative insights about how the flapping process of the laminar separation bubble within the boundary layer near the trailing edge affects the aerofoil self-noise. It is found that the aerofoil A7 with smooth curvature distributions presents a 10% smaller laminar separation bubble compared to the aerofoil E387 at Reynolds number 100,000 and Angle of Attack 4-degree. The LES results also suggests that curvature distribution smoothing leads to a 6.5% reduction in overall broadband noise level.

Originality/value – This paper fulfils an identified need to reveal the unknown flow structure and the boundary layer characteristics that resulted in the self-noise reduction phenomenon yielded by curvature distribution smoothing.

Keywords: Aerofoil self-noise, Surface curvature distribution, Large Eddy Simulation, Laminar separation bubble

Article Type: Research paper

NOMENCLATURE

Roman Symbols

a_0	The local speed of sound
c	Chord length of an aerofoil
C_d	Drag coefficient
C_p	Pressure coefficient
E	Energy of a signal in signal processing
$f^{-5/3}$	The $-\frac{5}{3}$ Kolmogorov spectrum
L_p	Sound pressure level (SPL)
M	Mach number
p	Pressure
r	The distance between the receiver and the source
Re	Reynolds number
St	Strouhal number
S_{wall}	The surface area of the aerofoil section
T	Estimated period of vortex shedding
(u,v,w)	Velocity components in three dimensions
U	Free stream velocity
(x,y,z)	Cartesian coordinates
x_i	The location of the receiver, i is 1 or 2, denoting the streamwise and crossflow direction components respectively
y	The location of the sound source
y^+	Dimensionless height of the first cell to the surface

Abbreviations

AoA	Angle of Attack
IB	Immersed Boundary
LE	Leading Edge
LES	Large Eddy Simulation
LSB	Laminar Separation Bubble
QMUL	Queen Mary University of London
RANS	Reynolds-averaged Navier-Stokes
SPL	Sound Pressure Level
TE	Trailing Edge

1. INTRODUCTION

Surface curvature distribution is a relatively new topic in aerofoil designs used in external devices, although it has been proved that smooth curvature distributions are beneficial to the performance of turbomachinery blades. Many conventional aerofoils present unsmooth curvature distributions, particularly at the point where the leading edge (LE) joins the main part of the aerofoil. Unlike the existence of surface roughness, these unsmooth parts in the distribution of surface curvature are invisible to the observer in the aerofoil shapes, but they produce unusual loads [1, 2], higher aerodynamic drag [3-5] and louder aerofoil self-noise[6, 7].

On low Reynolds number aerofoils, it is found that continuous and smooth curvature distributions have impacts on the behaviour of the boundary layer on an aerofoil by affecting the size and the position of the laminar separation bubble (LSB) [8, 9]. Although there are different proposed mechanisms regarding the generation of tonal noise, it is agreed that a necessary condition for acoustic tones is that the LSB is adequately close to the trailing edge (TE) of the aerofoil [10], i.e., the position of laminar-turbulent transition must be sufficiently downstream so the large scales in the flow can be presented near the TE. However, the existing research into the tonal noise mechanisms is mainly limited to symmetric aerofoils, especially NACA0012, without considering the influence from the aerofoil camber which could also contribute to the tonal noise phenomenon on asymmetric aerofoils such as E387. Moreover, the main feedback loop relates to the LSB on the pressure surface of a symmetric aerofoil, but an asymmetric aerofoil may not exhibit a LSB on the pressure surface at a low Reynolds number [11, 12].

Figure 1. Profile geometries of the original aerofoil E387 and the redesigned aerofoil A7 (top) and their curvature distributions (bottom). The subfigure is the magnification of the curvature distribution at the LE area.
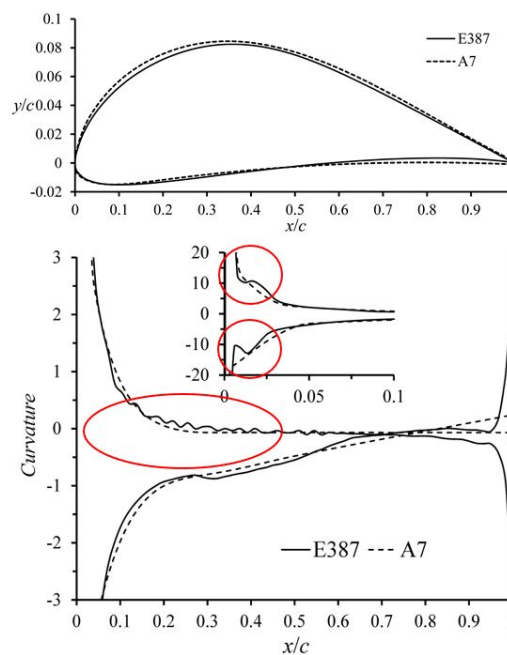
In previous studies [6, 8, 13, 14] the aerofoil E387 has been redesigned by removing the irregularities from the surface slope-of-curvature distribution from the LE to the TE and the redesigned aerofoil is denoted as "A7", as presented in Figure 1. Experimental work proved that the redesigned aerofoil has improved time-averaged aerodynamic performance at low Reynolds numbers. By redesigning the aerofoil E387 with smooth curvature distributions, aerodynamic drag can be reduced at low angles of attack (AoAs) and the stalling angle can be increased. Aeroacoustic wind tunnel measurements suggested that the redesigned aerofoil A7 showed noticeable reduction of self-noise by 7 dB in sideway propagations at the Reynolds number 100,000. However, the flow structure and the boundary layer characteristics that resulted in this self-noise reduction phenomenon remain unknown, which makes the time resolved flow field of both aerofoils essential to be simulated to analyse the aerodynamic mechanisms leading to improved performance yielded by the smooth curvature distribution.

In this paper, Large Eddy Simulations (LES) are conducted to further investigate the unsteady performance of both original aerofoil E387 and redesigned aerofoil A7 in a time-dependent study of the boundary layer characteristics. The positions of LSBs, spectra of the vertical fluctuating velocity component, flow vorticity and spectra plots within the upper surface boundary layer at the trailing edge, along with the wake profiles of mean streamwise velocity will be presented and analysed in-depth. The driven mechanisms of reducing aerofoil self-noise with smooth curvature distributions will be unveiled and discussed in detail.

2. FLOW SIMULATION METHODOLOGY

In this study, an in-house code of Queen Mary University of London (QMUL) called CgLes is utilised to simulate the flow over both aerofoils. The computational domain including the boundary conditions is presented in Figure 2. As a highly parallelized and efficient CFD code, CgLes was conducted on the UK national supercomputing service ARCHER. It has recently been updated with a novel iterative direct-forcing method [15]. The code is governed by incompressible three-dimensional Navier-Stokes equations which are discretized on a fixed staggered Cartesian grid and solved by the finite volume approach. A third order Runge-Kutta explicit method is used for time stepping scheme.

2.1 Numerical setup

Inagaki's Mixed Time Scale (MTS) model is used as the subgrid-scale model in current simulations due to its capability to accurately predict the pressure fluctuations on the aerofoil surface at $Re = 10^4 \sim 10^5$ [16]. Unlike the Smagorinsky model, the MTS subgrid-scale model does not require a wall damping function because the velocity scale close to zero and the time scale is guaranteed to have smaller scales in near wall region. The MTS model constant C_{MTS} is set to 0.05, and another model constant C_T in the time scale determination is set to 10.0. The immersed boundary (IB) points are used to represent the aerofoil, based on a novel direct forcing IB method with an improved body force distribution scheme [17].

It is worth to mention that the MTS subgrid-scale model is not a hybrid model and consequently no RANS turbulence model is solved for the near-wall problem. It has shown significant advantages in accurately predicting the near-wall pressure and velocity fluctuations compared to RANS turbulence models, making it an ideal option to conduct aerodynamic noise predictions. Similar to scaling the flow parameters in wind tunnel experiments, scaling the parameter dimensions in Navier-Stokes equations can offer more profound understanding of the studied case, in addition to decrease the parameter numbers in the equations. In this study, parameters such as spatial coordinates, velocity, chord length and pressure, are normalised. A fully non-dimensional momentum equation is used for all the simulations with a dimensionless viscosity $\nu^* = \nu/(U_\infty c)$. In order to reach $Re = 10^5$ in reality, corresponding experimental parameters U_∞ and c are used to determine the dimensionless viscosity ν^*. The turbulence intensity at both the inlet and the outlet is set to 0.5%.

2.2 Mesh refinement in the LE and TE regions

In previous studies of CgLes [15], a uniform mesh was applied to the aerofoil proximity for higher simulation accuracy. It was found that the predictions of lift and drag force became inaccurate as the AoA increased. This is because the uniform mesh in the aerofoil vicinity cannot accurately capture the flow field characteristics, especially in the LE and TE regions where the curvature variations are very large compared to those in the main body region. To precisely simulate the LE and TE regions, the local mesh has to be refined properly. However, when using a uniform refinement, the refined grids of the LE and TE region will cause the meshes in other regions to be over-refined. In other words, if one is using a uniform mesh in the proximity of the whole aerofoil, the appropriate mesh scale for the main body region is not suitable for the LE and TE region but refining the mesh globally will significantly and unnecessarily increase the computational cost of the whole domain.
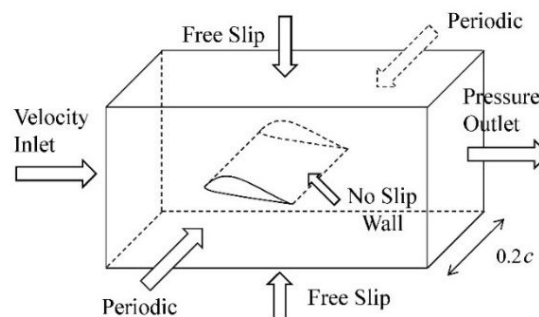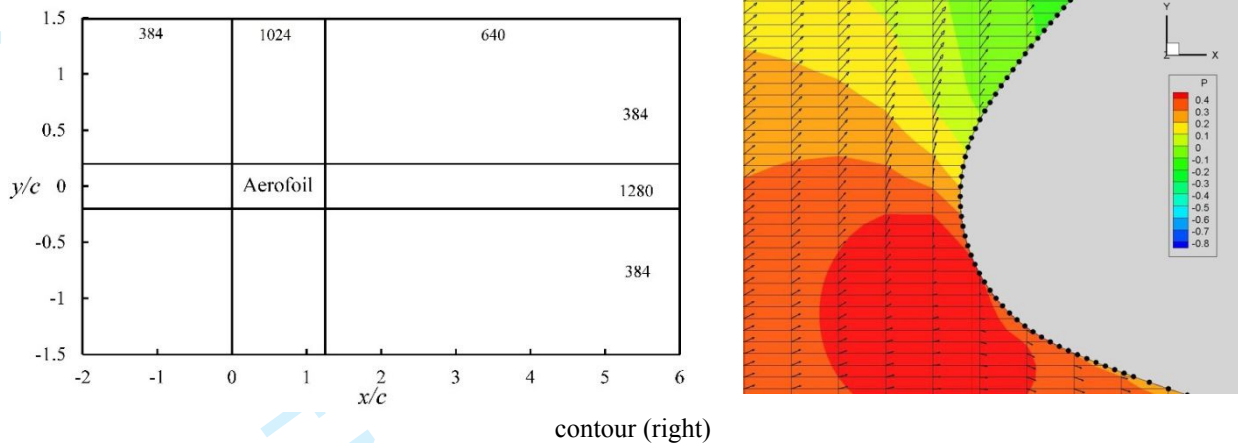

Figure 2. The schematic description of the computational domain and the boundary conditions

Figure 3. The XY plane cell distribution in computational domain (left) and LE IB points distribution in pressure

contour (right)

To overcome this known drawback, the streamwise grids in the proximity of the aerofoil are reconstructed based on the uniform mesh. The streamwise grids in the LE region ($0 \leq x/c \leq 0.02$) are refined by three times and the grids outside the LE region are stretched until the streamwise grid length return to the uniform size. The same refinement is also used for TE region. The cell distribution and the Cartesian grids in the proximity of the LE is shown in Figure 3. Between neighbouring grid cells, the increase ratio of the grid length remains lower than 1.03. The conventional y+ in conformal mesh needs to be considered along with x+ in Cartesian grids, especially for the LE and TE region due to the fact that the Cartesian grids are not conforming to the aerofoil surface. This is similar to the study of Eisenbach et al. [18] who used d+ to verify that the grid points are close enough to aerofoil surface. In this way we refine the streamwise computational mesh in the proximity of the aerofoil, ensuring x+ < 2 for the nose region in the leading edge. It has to be noted that the real x+ and y+ for the aerofoil model are smaller than the estimations based on the Cartesian grids because the IB points (aerofoil) are usually inside the grid cells.

The mesh in the LE region is hence refined by the cell reconstruction, while the mesh in the main body region remains uniform. The simulated pressure coefficients are compared in Figure 4. The simulation with uniform grids could not accurately predict the pressure coefficients at position $0 \leq x/c \leq 0.02$, as presented in Figure 4(left). More precisely, it underestimated the Cp magnitude by 60% as it did not capture the LE short bubble on the suction side. The prediction on the pressure side is more accurate than that on the suction side, and the uniform mesh in the proximity of the aerofoil resulted in a 15% underestimation of Cp at position $0 \leq x/c \leq 0.05$. Despite the inaccuracies at the LE region, the simulation with uniform grids offers good agreement with the experimental data. In Figure 4(right) the results simulated with reconstructed grids provide good agreement with the experimental results. The refinement of the LE region significantly increased the accuracy of Cp prediction at the LE region compared to the uniform grids. Therefore, the reconstructed grids near aerofoil surface are used in the simulations.
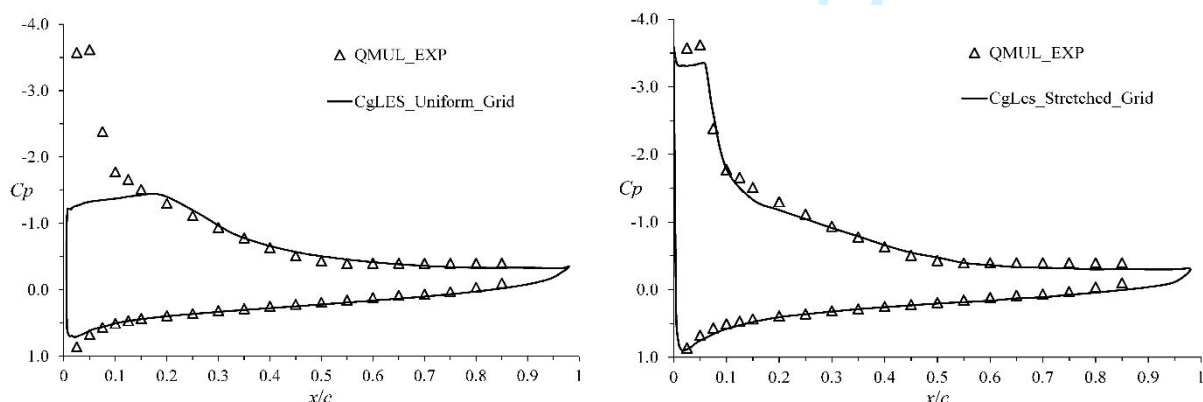
Figure 4. Comparison of the pressure coefficients simulated using the original uniform mesh (left) and reconstructed stretched mesh (right) in the proximity of the aerofoil A7 at AoA= 14-deg and Re = 10^5.

2.3 Aeroacoustic predictions
The flow field of each aerofoil is simulated by LES, and subsequently the Lighthill-Curle acoustic analogy is used to

calculate the generated sound. Here we follow the method of Suponitsky et al. [19] and consider that generated aerofoil self-noise results primarily from dipole contribution. In the present incompressible calculations, the aerofoil is considered as a compact source due to the nearly zero Mach number $M \ll 1$. Hence the time variations of the source have a wavelength λ approaching infinity, i.e., $\lambda = c \cdot M^{-1} \gg 1$, where c is the chord length of the aerofoil. The compact aerofoil acts as a dipole in the streamwise and spanwise directions, and the far-field pressure in the compact limit is given in Howe's work [20]:

$$p'(x,t) = \frac{x_i}{2\pi a_0 r^2} \int_{S_{wall}} \frac{\partial p}{\partial t}\left(y,t - \frac{x}{a_0}\right) dS_i(y)$$

(1)

where x is the location of the receiver, i is 1 or 3, denoting the streamwise and spanwise direction components respectively, r is the distance between the receiver and the source, p is the computed local pressure on the aerofoil surface as in [19], a_0 is the local speed of sound, y is the location of the source, and S_{wall} is the surface area of the aerofoil section. Eq. 1 indicates that the compact far-field pressure is proportional to the time derivative of the lift and drag experienced by the aerofoil.

The sound pressure level (SPL) is made on a logarithmic scale due to the wide range of the sound, and it can be calculated from:

$$L_p = 20 log_{10}\left(\frac{p_{rms}}{p_0}\right) \quad dB$$

(2)

where L_p denotes SPL, p_{rms} denotes the root mean square of sound pressure and p_0 denotes the reference sound pressure in air which commonly refers to the threshold of hearing: 2×10^{-5} Pa.

3. RESULTS AND ANALYSIS

Although LES requires less computational resources than DNS, the requirement for small time-steps and the three-dimensional grids make the current LES considerably computational expensive. Unlike RANS computations, the experimental operating conditions cannot be replicated for all cases with LES due to the computational cost. Instead, a representative angle of attack 4-deg for both aerofoils at Re = 100,000 is selected for each aerofoil as a compromise, intended to present detailed investigations into the mechanisms behind tonal noise with limited computational resources.

The results are compared with experimental data which were obtained by wind tunnel measurements to the original aerofoil E387 and the redesigned aerofoil A7 at chord-length based Reynolds number 100,000, 200,000 and 300,000 to investigate their aerodynamic and aeroacoustic performance at different AoAs. The aerodynamic benchmarking experiments were carried out in QMUL No.2 subsonic wind tunnel which is a closed-circuit type with a 5.6:1 contraction ratio, while the benchmarking aeroacoustic experiments were conducted in BUAA D5 subsonic closed-circuit type wind tunnel with an anechoic chamber. More specific details are demonstrated in Ref [6, 14].

The simulated results of mean pressure coefficients of both aerofoils are presented in Figure 5. Generally the LES reproduced the experimental Cp distributions for both aerofoils. On the suction sides, E387 reaches its lowest Cp of -1.07 at the position x/c = 0.055 while A7 provides its lowest Cp of -1.12 at the position x/c = 0.078. The aerofoil A7 with smooth curvature distributions offers lower Cp at the suction side before the laminar-turbulent transition, particularly at the position $0.05 < x/c < 0.2$ where an obvious slope-of-curvature irregularity is fixed, as shown in Figure 1. A pressure plateau is reached at position x/c = 0.4 for each aerofoil, indicating the laminar separation position of the LSB. The LES results slightly overestimated the position of the end of the pressure plateau for each aerofoil, resulting in overestimating the LSB sizes of both aerofoils by approximately 5%. The mean pressure coefficients indicate that A7 has a 10% smaller size of LSB than E387 due to the different flow transition positions and turbulent re-attachment positions. On the pressure sides, both aerofoils present similar Cp distributions.
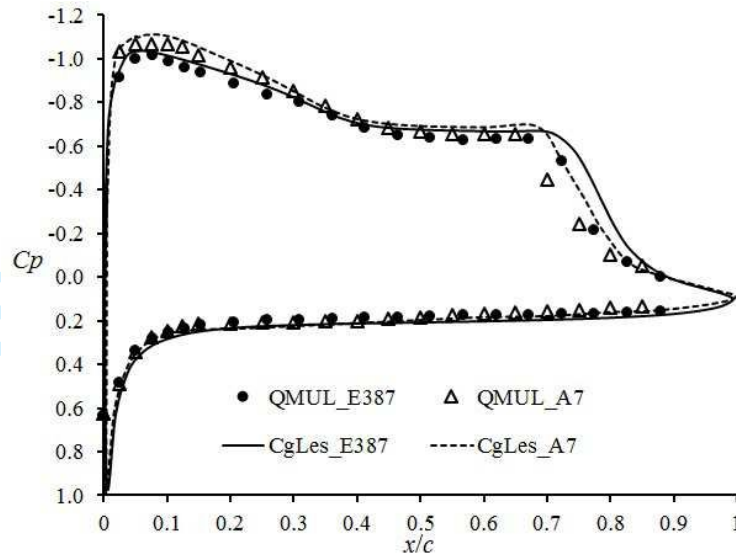
Figure 5. Pressure coefficient distribution at 4-deg AoA, Re=100,000 from LES results and the experiments

Table 1. Time-averaged lift and drag coefficients for LES and experimental results

Cl	Exp	LES	Error
E387	0.785	0.806	2.61%
A7	0.782	0.802	2.49%
Cd	Exp	LES	Error
E387	0.0242	0.0281	13.88%
A7	0.0223	0.0255	12.55%

The time-averaged lift and drag coefficients obtained from the simulations are compared with the experimental results, as shown in Table 1. The LES results matched the experimental data. The mean Cl of both aerofoils are slightly overestimated by the simulations compared to the experimental results. This is due to the overestimation of the LSB size for each aerofoil, leading to more downstream positions of the laminar-turbulent transition and the turbulent re-attachment, and hence resulting in higher time-averaged lift and drag coefficients. It is not surprising that the effects of the bubble-size overestimation are more significant on the mean Cd predictions, because the LSB dominates the aerofoil performance at the current Reynolds number and the LSB affects the drag performance more than the lift performance. The simulation of A7 predicts a very similar Cl magnitude compared to E387, which is consistent with the experimental data. The predicted Cd magnitude of A7 is 9.2% smaller than that of E387 because of the smaller LSB size.
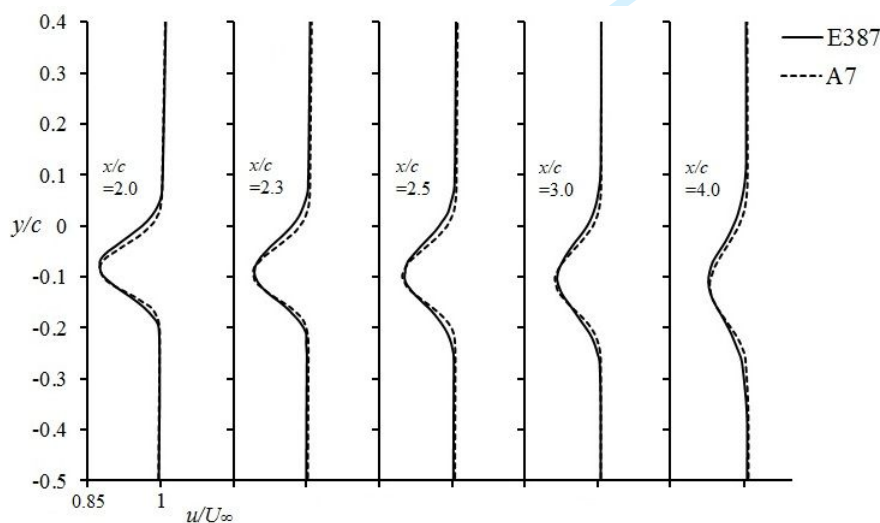

Figure 6. Wake profiles of mean streamwise velocity. The five curves in the plot correspond to the wake positions x/c = 2, 2.3, 2.5, 3.0 and 4.0 respectively, from left to right.

A more detailed comparison of the wake velocity profiles between these two aerofoils at five different wake stations is presented in Figure 6, which shows the different streamwise velocity recovery processes observed in the simulated wake for the two aerofoils. Setting the coordinate $(0.25c, 0)$ as the aerodynamic centre of the aerofoil (the same point based on which the aerofoil is rotated to vary the AoA), the five wake positions range from one to three chord length away from the trailing edge. At these five positions, each aerofoil presents the same maximum velocity deficit value but A7 has a narrower velocity deficit region than E387, resulting in a lower Cd.

Spectral analysis of velocity time histories in the boundary layer of each aerofoil was conducted to investigate the flow structures and the corresponding characteristics. The power spectrums of crossflow direction velocity fluctuations of both aerofoils are presented in Figure 7. The spectra were determined by applying a fast Fourier transform to the velocity fluctuation signals. At each streamwise sampling position, the velocity signal was monitored in the aerofoil boundary layer, at the vertical position where the velocity is half the velocity at the boundary layer edge. This position is selected because it corresponds to the maximum root-mean-square velocity in the boundary layer, and consequently is the position where the velocity spectra can be presented most accurately.
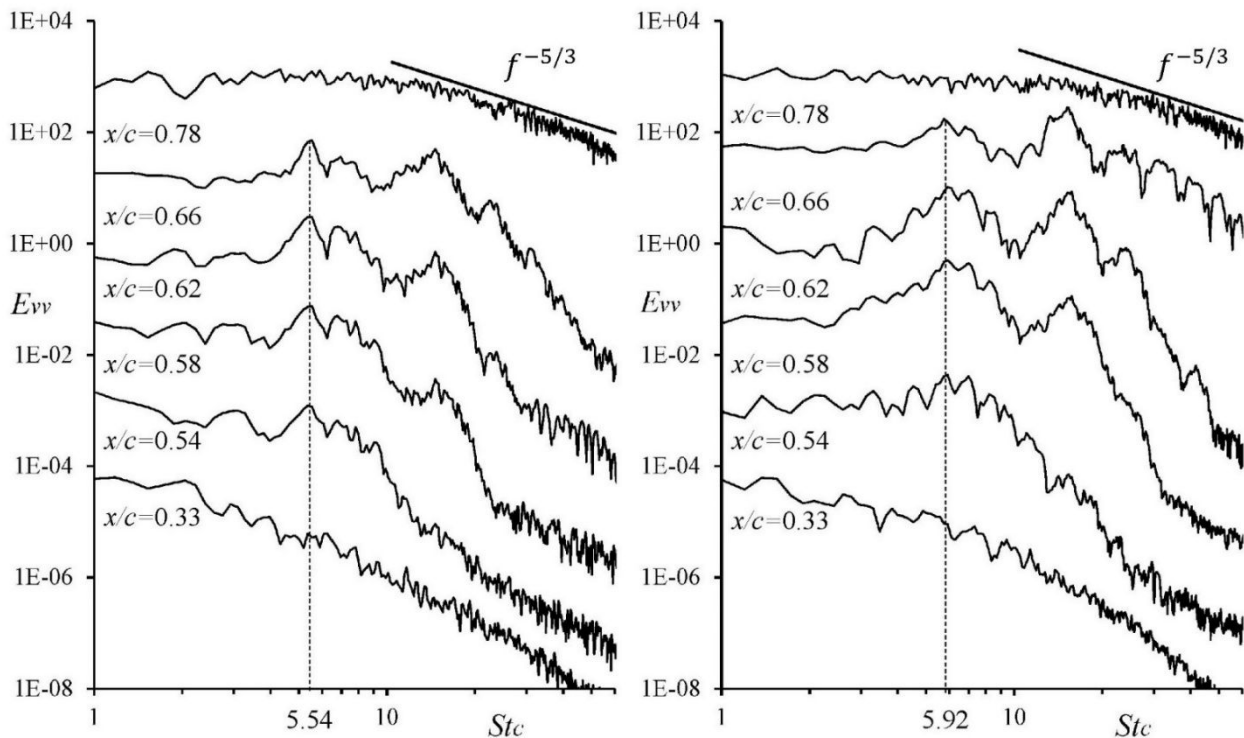

Figure 7: Spectra of the vertical fluctuating velocity component for aerofoil E387 (left) and A7 (right) at 4-deg AoA, Re=100,000. The amplitude of each successive spectrum is stepped by one order of magnitude.

Figure 7 shows the spectra of the vertical velocity in the separated shear layer on the suction surface at 4-deg AoA and Re=100,000, depicting the process of laminar-turbulent transition for both aerofoils. The streamwise locations of the monitoring points are presented in the figure, and the spectrum amplitude of the adjacent monitoring points are stepped by one order of magnitude for clarity purpose. A similar transition process is found in the simulations for both aerofoils.

A fundamental frequency is found for each aerofoil in the separated shear layer, and the corresponding Strouhal numbers based on the chord length are 5.54 and 5.92 for E387 and A7 respectively. Representing the ratio of inertial forces due to the local acceleration of the flow to the inertial forces due to the convective acceleration, the Strouhal number based on the chord length St_c can be expressed as

$$St_c = \frac{fc}{U}, \tag{3}$$

where f is the frequency of vortex shedding, c is the chord length and U is the flow velocity.

The vortex shedding frequency results of E387 are consistent with the unsteady RANS computations of Lin et al. [21].

For each aerofoil, the disturbances growth is observed at position x/c = 0.54. Subsequently the fundamental frequency presents the initiation and development of harmonics, shortly followed by laminar-turbulent transition and the turbulent re-attachment. At streamwise position x/c = 0.66, the transition process is observed on aerofoil A7 due to its more energetic power spectrum, while on E387 the disturbances are still in the process of growing and developing. This again indicates a longer LSB on E387 due to the delayed transition and turbulent re-attachment positions. For both aerofoils a typical turbulence spectrum is found at the streamwise position x/c = 0.78, indicating the transition process is complete and the velocity at this position is in the turbulent boundary layer.
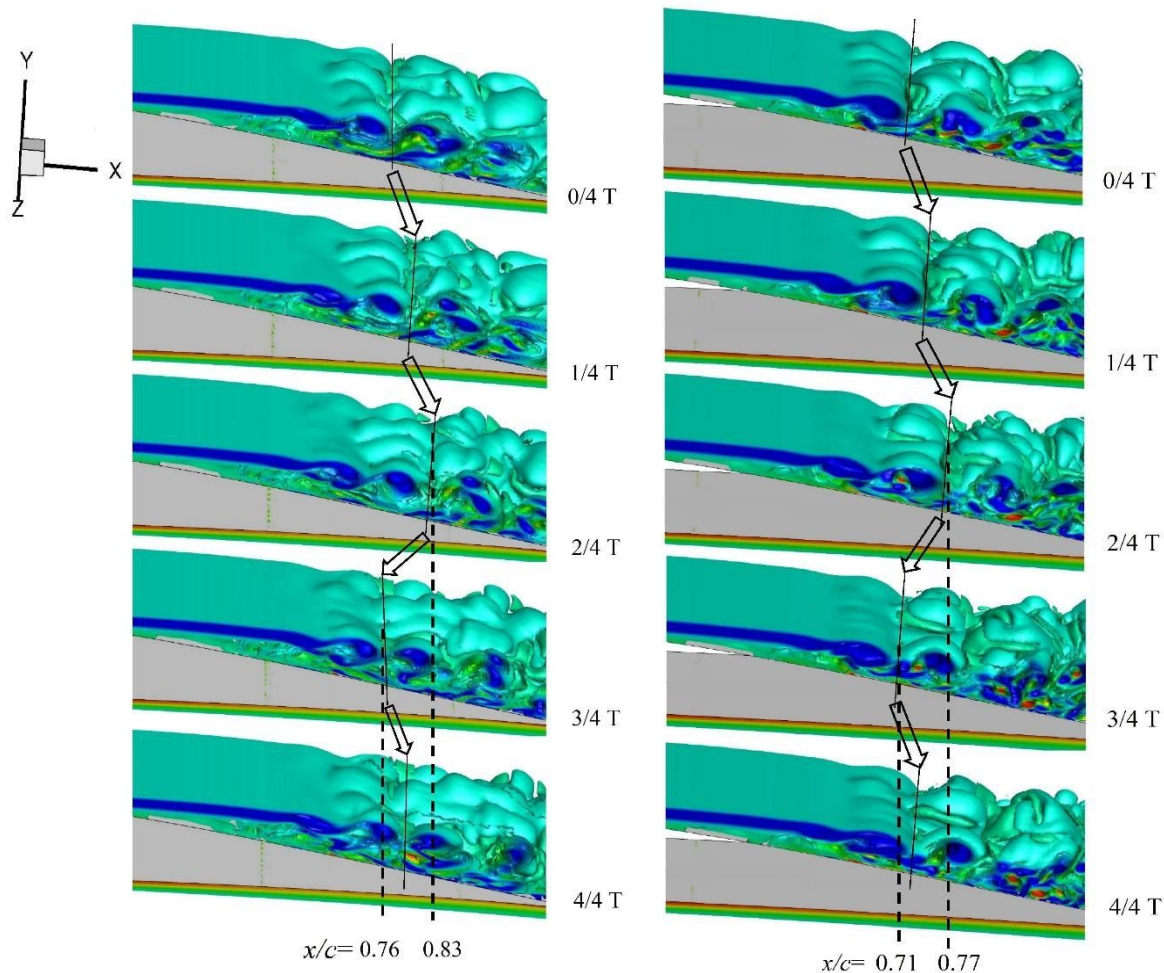

Figure 8: Vorticity contours of the aerofoil E387 (left) and A7 (right) at 4-deg AoA and Re=100,000.
The solid lines are the instantaneous turbulent reattachment positions of the LSB.
The dash lines in each figure indicate the bubble flapping range in a vortex shedding period

The fundamental frequencies observed in Figure 7 are used to estimate the vortex shedding period for both aerofoils, and the vorticity contours in a cycle of each aerofoil at 4-deg AoA and Re=100,000. are presented in Figure 8 for 5 equally spaced time intervals. The phenomenon of LSB flapping, which is believed to be an essential reason for the trailing edge tonal noise, is observed for both aerofoils. The process of the bubble flapping can be summarised as three steps: developing, detachment, and redeveloping. During the phase 0/4 T on the aerofoil E387, a spanwise vortex within the separation bubble is observed. The vortex develops and moves downstream during the phases 1/4 T and 2/4 T. It develops to a critical size and subsequently detaches from the leading primary separation between 2/4 T and 3/4 T. Consequently, the original LSB is divided into two separated portions, as shown in phase 3/4 T, and the detached vortex moves downstream, known as 'vortex shedding. During the detachment process of the vortex from 0/4 T to 3/4 T, new disturbances grow and develop into a new vortex. At the phase of 4/4 T this new vortex meets a similar status of the detached vortex at the phase of 0/4 T, and the redevelopment of a new vortex in the remaining separation bubble starts.

This cycle is considered as a single period of the LSB flapping mechanism.

As shown in the vorticity contours, the flow is steadier at the front part of the LSB compared to the vortex forming region. The more energetic fluid indicates higher momentum in the downstream region where the vortex is being shed. The trailing position of an undetached vortex in the separation bubble is regarded as the instantaneous position of the turbulent re-attachment, shown as solid lines in Figure 8. The arrows illustrate the position variations of the bubble reattachment for each aerofoil. It is observed that the instantaneous re-attachment position of the bubble on E387 flapped from x/c = 0.76 to 0.83 in a cycle for the five presented time intervals, as indicated with the dashed lines. The aerofoil A7 exhibits a similar 'developing–detachment–redeveloping' process of LSB flapping and vortex shedding as the aerofoil E387, although the instantaneous position of the turbulent re-attachment on A7 is typically further upstream compared to those on E387. For the five presented intervals the instantaneous re-attachment position of the bubble on A7 varies from x/c = 0.71 to 0.77, further corroborating with the presented evidence of a smaller size LSB on A7 than on E387. At the current Reynolds number Re = 100,000, the LSB size dominates the aerofoil performance, especially the drag performance. The slope-of-curvature irregularities cause more downstream transition and re-attachment positions and hence larger bubble size on the aerofoil E387, leading to larger scales in the flow passing the TE. The transition process adequately in proximity of the TE is believed to be a necessary condition to generate a pronounced tonal energy content [10, 22].

The time history of the pressure fluctuations at the trailing edge of each aerofoil at 4-deg AoA and Re = 1×10^5 was monitored within the aerofoil boundary layer, using the same method as described the velocity signal monitoring to determine the vertical monitoring position. The pressure power spectra are computed as shown in Figure 9, describing the frequency content of the TE noise including the tonal noise. The horizontal axis is converted to Strouhal number in order to perform non-dimensional analysis and compare the simulation with the experimental data. The resolution of the frequency domain Δf is 0.125, and the spectra have been compared with higher and lower frequency resolution to ensure the desired signals are not neglected or affected by the numerical noises.

It is convenient to provide a measure of the overall acoustic noise intensity: the overall sound pressure level (OASPL), which can be calculated from integrating over the entire frequency range in a SPL spectrum. It is found that the OASPL of E387 and A7 is 47.6 dB and 44.5 dB. The smooth curvature distributions result in fewer significant fluctuations in the time derivative of the aerodynamic forces, leading to a 3.1 dB reduction in overall broadband noise level on A7 compared to E387.

Figure 9 shows that for both aerofoils the flow fields present broadband contents to the TE noise. A dominant narrowband tone is observed at St_c = 6.44 in the aerofoil boundary layer of E387. This primary tone is found to be composed of a single peak, and a higher harmonic is observed at $St_c \approx 9.0$. The peak frequency of the primary tone in the SPL spectrum for E387 at AoA = 4-deg which is presented in [14] is 182 Hz, and the corresponding Strouhal number is St_c = 6.4. It is apparent that the corresponding Strouhal number of the primary tonal frequency in the SPL spectrum is approximately the same as the Strouhal number of the dominant tone in the pressure fluctuation spectrum in the boundary layer near the trailing edge. This phenomenon was also observed in the study by Arbey and Bataille [23], further validating the simulation accuracy. A less significant tone in terms of amplitude on the aerofoil A7 can be found at $St_c \approx 5.0$. Although this Strouhal number meets the corresponding Strouhal number of the primary tonal frequency in the SPL spectrum in [14], the tone is too weak to be observed with respect to the broadband noise. This very weak tone on A7 is expected, because the primary tone itself at 146 Hz in the experimental results in [14] is discerned to be so weak that it can be easily neglected in the spectra of lower frequency resolution. Moreover, the aerofoil tone phenomenon was proved to be very complicated and difficult to predict [10] as it requires accurate simulations on flow separation, hydrodynamic disturbance growth and even acoustic sound wave generation and propagation. The overall broadband noise of E387 is greater than that of A7, because of the differences of the LSB sizes and transition positions on two aerofoils as previously described. Due to its transition positions further downstream, the flow near the TE of E387 contains larger scale coherent structures which appear to be more energetic and more possibly be promoted to acoustic tonal behaviour.
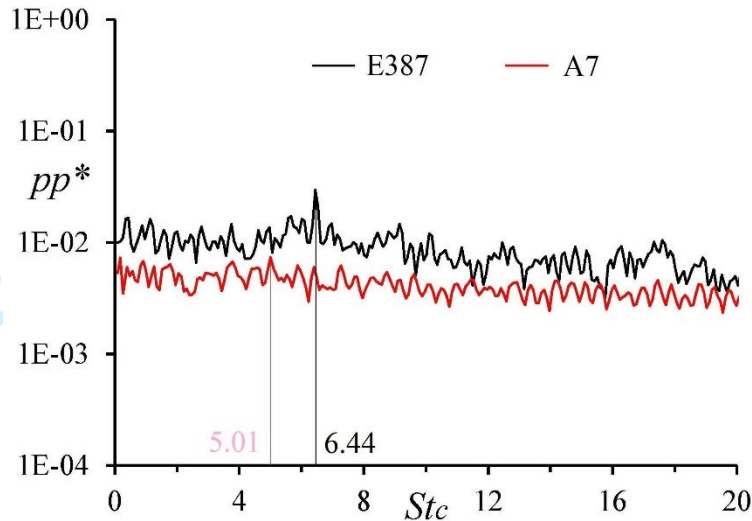
Figure 9: Pressure power spectra computed within the upper surface boundary layer at the trailing edge for each aerofoil at AoA = 4-deg and Re = 1×10^5. *Stc* denotes Strouhal number based on the chord length

To quantitatively investigate the effects of surface slope-of-curvature irregularities on the self-noise levels of the aerofoil, the farfield pressure fluctuations are estimated with Eq. 1 and the SPL spectra of both aerofoils are calculated with Eq. 2. The results are shown in Figure 10. It must be noted that it is meaningless to directly compare the numerical SPL spectra with the broadband spectra of the experimental results because of the effects of the background noise of the wind tunnel. Nevertheless, the characteristics of the tonal noise from the experimental work provide references for the current numerical study.

Figure 10: The LES results of the noise level spectra for the both aerofoils at AoA = 4-deg and Re = 1×10^5. The upper
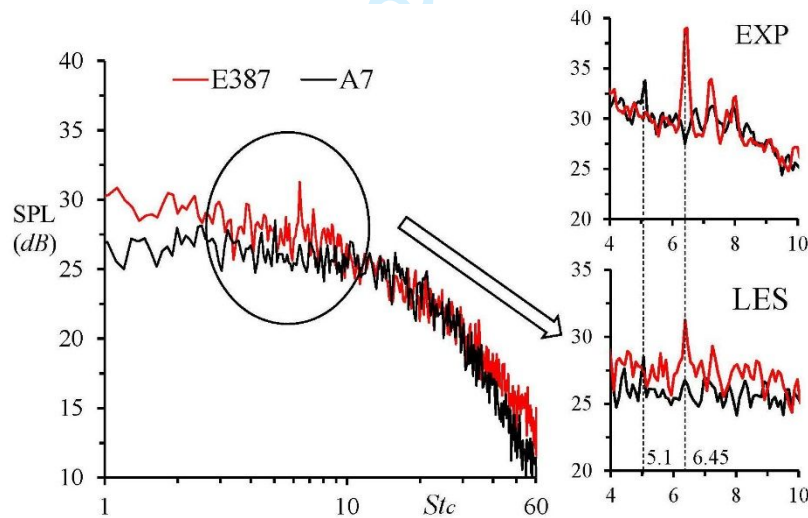
and lower sub-figures are magnified views of the experimental and numerical SPL spectra respectively in the vicinity of the dominant tones. Both experimental and numerical results are considered at 10 chord lengths away from the trailing edges [6].

Similar to the pressure spectrum, a single primary tone is observed in the SPL spectrum of the aerofoil E387. The corresponding Strouhal number is found to be 6.45 in the magnified view in Figure 10. It is consistent with the Strouhal number of the dominant tonal peak in the experimental results as shown in the upper and lower sub-figure, and consistent with the primary peak in the pressure spectrum shown in Figure 9, i.e., the same peak frequency described by Arbey and Bataille [23]. The excellent agreement between the simulations and the experiments in terms of the dominant frequencies further validate the adequacy of the computational grid. The SPL magnitude of the simulated primary tone is 5 dB smaller than in the experimental data, probably due to the existence of background noise of the wind tunnel experiments. Another possible reason is the instinctive characteristic of LES as a subgrid model is used in LES to model the small scales in the

flow. Modelling small scales in LES can cause the pressure fluctuations to be underestimated [24], leading to a lower SPL estimation. It is difficult to discern a primary tone in the SPL spectrum of the aerofoil A7 with respect to the broadband noise. In the magnified sub-figure, a weak tone is detectable at $St_c \approx 5.0$ which is consistent with the experimental results and the numerical pressure spectrum.

It is convenient to provide a measure of the overall acoustic noise intensity: the overall sound pressure level (OASPL), which can be calculated from integrating over the entire frequency range in a SPL spectrum. It is found that the OASPL of E387 and A7 is 47.6 dB and 44.5 dB. The continuous slope-of-curvature irregularities result in fewer significant fluctuations in the time derivative of the aerodynamic forces, leading to a 3.1 dB reduction in overall broadband noise level on A7 compared to E387.

4. CONCLUDING REMARKS

The impacts of smooth surface curvature distributions are taken into consideration to investigate their effects on aerofoil tonal noise phenomenon. The aerofoil Eppler 387 was redesigned by removing the irregularities in surface slope-of-curvature distributions and the redesign aerofoil is denoted as "A7". Three-dimensional LES was performed on both aerofoils to further investigate the unsteady performance of each aerofoil. A larger laminar separation bubble is found on the aerofoil with slope-of-curvature irregularities at 4-deg AoA and Re=100,000. In a time-dependent study of the boundary layer characteristics on both aerofoils, it is found that they share nearly identical laminar separation positions while the turbulent re-attachment position of E387 is further downstream compared to A7, causing bubble flapping positions closer to the trailing edge, which resulted in a more significant tone in the pressure spectra monitored within the boundary layer of the TE of the aerofoil. The LES results also showed a 6.5% reduction in overall broadband noise level on A7 with smooth curvature distributions compared to the original aerofoil E387.

5. ACKNOWLEDGMENTS

6. REFERENCES

[1]   I. Hamakhan and T. Korakianitis, "Aerodynamic performance effects of leading-edge geometry in gas-turbine blades," *Applied Energy,* vol. 87, no. 5, pp. 1591-1601, 2010.

[2]   T. Korakianitis, I. Hamakhan, M. Rezaienia, A. Wheeler, E. Avital, and J. Williams, "Design of high-efficiency turbomachinery blades for energy conversion devices with the three-dimensional prescribed surface curvature distribution blade design (CIRCLE) method," *applied Energy,* vol. 89, no. 1, pp. 215-227, 2012.

[3]   Y. Song, C.-W. Gu, and Y.-B. Xiao, "Numerical and theoretical investigations concerning the continuous-surface-curvature effect in compressor blades," *Energies,* vol. 7, no. 12, pp. 8150-8177, 2014.

[4]   T. Korakianitis, M. Rezaienia, I. Hamakhan, and A. Wheeler, "Two-and three-dimensional prescribed surface curvature distribution blade design (CIRCLE) method for the design of high efficiency turbines, compressors, and isolated airfoils," *Journal of turbomachinery,* vol. 135, no. 4, p. 041002, 2013.

[5]   K. Ai, E. Avital, X. Shen, A. Samad, and N. Venkatesan, "The surface curvature effect on performance of a laboratory scale tidal turbine," in *The World Congress on Engineering*, 2018: Springer, pp. 101-113.

[6]   X. Shen *et al.*, "Surface curvature effects on the tonal noise performance of a low Reynolds number aerofoil," *Applied Acoustics,* vol. 125, pp. 34-40, 2017.

[7]   D. J. Moreau, T. F. Geyer, C. J. Doolan, and E. Sarradj, "Surface curvature effects on the tonal noise of a wall-mounted finite airfoil," *The Journal of the Acoustical Society of America,* vol. 143, no. 6, pp. 3460-3473, 2018.

[8]   X. Shen, E. Avital, M. A. Rezaienia, G. Paul, and T. Korakianitis, "Computational methods for investigation of surface curvature effects on airfoil boundary layer behavior," *Journal of Algorithms & Computational Technology,* vol. 11, no. 1, pp. 68-82, 2017.

[9]   Z. Yang and P. R. Voke, "Large-eddy simulation of boundary-layer separation and transition at a change of surface curvature," *Journal of Fluid Mechanics,* vol. 439, pp. 305-333, 2001.

[10]   L. E. Jones and R. D. Sandberg, "Numerical analysis of tonal airfoil self-noise and acoustic feedback-loops," *Journal of Sound and Vibration,* vol. 330, no. 25, pp. 6137-6152, 2011.

[11]   M. S. Selig, *Summary of low speed airfoil data*. SOARTECH publications, 1995.

[12]   R. J. McGhee, *Experimental results for the Eppler 387 airfoil at low Reynolds numbers in the Langley low-turbulence pressure tunnel*. National Aeronautics and Space Administration, Scientific and Technical …, 1988.

1
2
3
4
5
6
7
8
9
10
11
12
13
14
15
16
17
18
19
20
21
22
23
24
25
26
27
28
29
30
31
32
33
34
35
36
37
38
39
40
41
42
43
44
45
46
47
48
49
50
51
52
53
54
55
56
57
58
59
60

[13]   X. Shen, T. Korakianitis, and E. Avital, "Numerical investigation of surface curvature effects on aerofoil aerodynamic performance," in *Applied Mechanics and Materials*, 2015, vol. 798: Trans Tech Publ, pp. 589-595.

[14]   X. Shen, E. Avital, G. Paul, M. A. Rezaienia, P. Wen, and T. Korakianitis, "Experimental study of surface curvature effects on aerodynamic performance of a low Reynolds number airfoil for use in small wind turbines," *Journal of Renewable and Sustainable Energy,* vol. 8, no. 5, p. 053303, 2016.

[15]   X. Bai, E. Avital, A. Munjiza, and J. Williams, "Numerical simulation of a marine current turbine in free surface flow," *Renewable Energy,* vol. 63, pp. 715-723, 2014.

[16]   M. Inagaki, T. Kondoh, and Y. Nagano, "A mixed-time-scale SGS model with fixed model-parameters for practical LES," *J. Fluids Eng.,* vol. 127, no. 1, pp. 1-13, 2005.

[17]   Z. Ikram, E. Avital, and J. Williams, "Detached eddy simulation of free-surface flow around a submerged submarine fairwater," *Journal of fluids engineering,* vol. 134, no. 6, 2012.

[18]   S. Eisenbach and R. Friedrich, "Large-eddy simulation of flow separation on an airfoil at a high angle of attack and Re= 105 using Cartesian grids," *Theoretical and Computational Fluid Dynamics,* vol. 22, no. 3, pp. 213-225, 2008.

[19]   V. Suponitsky, E. Avital, and M. Gaster, "On three-dimensionality and control of incompressible cavity flow," *Physics of Fluids,* vol. 17, no. 10, p. 104103, 2005.

[20]   M. Howe, "Edge, cavity and aperture tones at very low Mach numbers," *Journal of Fluid Mechanics,* vol. 330, pp. 61-84, 1997.

[21]   J. M. Lin and L. L. Pauley, "Low-Reynolds-number separation on an airfoil," *AIAA journal,* vol. 34, no. 8, pp. 1570-1577, 1996.

[22]   E. C. Nash, M. V. Lowson, and A. McAlpine, "Boundary-layer instability noise on aerofoils," *Journal of Fluid Mechanics,* vol. 382, pp. 27-61, 1999.

[23]   H. Arbey and J. Bataille, "Noise generated by airfoil profiles placed in a uniform laminar flow," *Journal of Fluid Mechanics,* vol. 134, pp. 33-47, 1983.

[24]   M. Wang, S. Moreau, G. Iaccarino, and M. Roger, "LES prediction of wall-pressure fluctuations and noise of a low-speed airfoil," *International journal of aeroacoustics,* vol. 8, no. 3, pp. 177-197, 2009.